Thermodynamic state variables in quasiequilibrium ultracold neutral plasma

Sanat Kumar Tiwari, Nathaniel R. Shaffer, and Scott D. Baalrud

Thermodynamic State Variables in Quasi-Equilibrium Ultracold Neutral Plasma

Sanat Kumar Tiwari,[1, *] Nathaniel R. Shaffer,[1] and Scott D. Baalrud[1]

[1]*Department of Physics and Astronomy, University of Iowa, Iowa City, Iowa 52242, USA*

(Dated: March 24, 2017)

The pressure and internal energy of an ultracold plasma in a state of quasi-equilibrium are evaluated using classical molecular dynamics simulations. Coulomb collapse is avoided by modeling electron-ion interactions using an attractive Coulomb potential with a repulsive core. We present a method to separate the contribution of classical bound states, which form due to recombination, from the contribution of free charges when evaluating these thermodynamic state variables. It is found that the contribution from free charges is independent of the choice of repulsive core lengthscale when it is sufficiently short-ranged. The partial pressure associated with the free charges is found to closely follow that of the one-component plasma model, reaching negative values at strong coupling, while the total system pressure remains positive. This pseudo-potential model is also applied to Debye-Hückel theory to describe the weakly coupled regime.

I. INTRODUCTION

Accurate models for the thermodynamic and transport properties of strongly coupled plasmas are essential for describing their evolution as a continuous fluid [1]. Ultracold neutral plasma (UCP) experiments provide an excellent test bed for validating such models because it is possible to precisely probe them using optical diagnostics in table-top experimental set-ups [2]. Verifying models using UCPs can also advance the understanding of other strongly coupled systems, such as high energy density plasmas [3–5], which arise in extreme environments and can be difficult to diagnose precisely. One of the most intriguing features is that UCPs are electron-ion systems in which each component can be in, or near, the strong coupling regime. Thus, they can provide insights into two-component physics beyond the reach of the common one-component plasma (OCP) approximation [6, 7]. In this paper, we develop a method to simulate an electron-ion plasma in a state of quasi-equilibrium using classical molecular dynamics (MD) simulations. This is applied to evaluate the pressure and internal energy of the system, as well as to distinguish the contributions from free charges and bound states [8]. These show that the free charge thermodynamics closely resemble predictions from the OCP model, but that classical bound states (analogous to the Rydberg atoms in an UCP) must also be accounted for to preserve physical limitations such as a positive total pressure.

UCPs are typically created by the photo-ionization of laser cooled atoms confined in a magneto-optical trap [9–11], and can have densities up to $10^{11} \mathrm{cm}^{-3}$. Ion temperatures at formation range from μK to mK, and the initial electron temperature typically ranges from 0.1-1 K. After formation, the plasma components are no longer confined, and the expansion has a cooling effect [12, 13].

However, this is overwhelmed by other heating mechanisms. Both ions and electrons are rapidly heated by disorder induced heating [14], and electrons are additionally heated by three-body recombination (3BR) throughout the plasma lifetime [15]. As a result, these are rapidly evolving, partially ionized plasmas with electrons in a weakly to moderately coupled state, and ions in a moderately to strongly coupled state. Previous simulation and modeling efforts have largely focused on describing the system evolution, including expansion, disorder induced heating, and eventual recombination to a collapsed neutral-like state [15–17].

Here, we instead focus on developing a method to study the properties of an UCP at fixed conditions, i.e., density and temperature. The motivation is to connect theories for thermodynamic and transport properties, which make predictions at fixed conditions, with experiments, which measure these properties over short enough time intervals that the conditions can be considered fixed. Experiments typically focus on measuring the free charges [2]. It is interesting from a theoretical viewpoint – and necessary for comparison with experiment – that one separates the bound state contributions from the free charge contributions when describing transport or thermodynamic properties. The primary challenge is that the equilibrium state of the system is a recombined neutral gas [15, 18, 19]. A successful model must somehow limit the recombination so that a free charge population remains, but do so in a way that one can connect that simulated equilibrium state with an interval of time during the evolution of the plasma in an experiment.

To accomplish this, we model electron-electron and ion-ion interactions with the Coulomb potential and electron-ion interactions with a pseudo Coulomb potential that also includes a repulsive core

$$v_{ee} = v_{ii} = \frac{e^2}{r} \tag{1a}$$

$$v_{ei} = -\frac{e^2}{r} \left[1 - \exp \left(-\frac{r^2}{(\alpha a)^2} \right) \right]. \tag{1b}$$

* sanat-tiwari@uiowa.edu

Here, r is the separation between two particles, e is the electron charge, $a = (3/4\pi n_i)^{1/3}$ is the average spacing between two ions or two electrons, n_i is the number density of ions with $n_e = n_i$, and α is an adjustable parameter that sets the e-i repulsion length scale. Simulations were conducted in a periodic box with both electrons and ions held to the same fixed temperature using a Nosé-Hoover thermostat [20]. Due to computing constraints, the ion mass was set to be 10 times the electron mass. Since mass does not influence the equilibrium properties of the system, which are the focus of this work, this reduced mass is inconsequential. Electrons are hotter than ions in real UCP experiments (ion coupling strength Γ_i up to 5 and electron coupling strength Γ_e up to 0.1), but we concentrate on equilibrium here because our interpretation of data will utilize aspects of equilibrium statistical mechanics. Future work will extend the model to treat unequal electron and ion temperatures.

The electron-ion potential in Eq. (1b) is similar to the Kelbg potential used to model dense, degenerate plasmas [21, 22]. However, an important difference arises here. In dense plasmas, the length scale αa is associated with the de Broglie wavelength characterizing quantum mechanical diffraction. At dense plasma conditions, the de Broglie wavelength is of the same order as the interparticle spacing, so αa is of order unity. As a result, α significantly influences the predicted thermodynamic properties and transport rates. In contrast, in a UCP the de Broglie wavelength is orders of magnitude smaller than a. In our model, α is a model parameter that does not represent a physical scale.

The main idea behind this model is that as α decreases, the properties of the free charge components of the system asymptote to values that are independent of α. Hence, these asymptotic values represent the state of the charged components at fixed conditions. The main result of this paper is the demonstration of this asymptotic plateau in the partial pressure and internal energy associated with the free charges as the parameter α is reduced. What does change as α shrinks is the fraction of the plasma in a bound state. Decreasing α increases the depth of the potential well in the electron-ion interaction, resulting in more classically bound pairs, or clusters. We observe that the bound state population has a lower temperature than the free population. This, along with a decreasing fraction of free charged states, leads to a slight slope in the thermodynamic variable profiles as α decreases. Nevertheless, the model provides a means to access properties of the charged particles (plasma) at fixed conditions via the asymptotic values obtained at small α, while also providing a means of controlling the bound state fraction. In essence, because it determines the bound state concentration(fraction), the value of the model parameter α provides a connection with a certain time interval of an ultracold plasma experiment.

Interpretation of the data requires a means to separate bound states from free charges. Here, we calculate the electron-electron, ion-ion and electron-ion radial distribution functions, $g_{ij}(r)$, and apply a simple model based on an energy argument to separate free and bound states. The pressure and internal energy are then computed directly from the radial distribution functions. The results provide a proof of principle of this technique. Future developments may address methods to directly separate free and bound states in the simulations, as well as to treat non-equilibrium systems that more closely represent experimental conditions.

This paper is organized as follows. Section II applies the model to Deybe-Hückel theory, which treats weakly coupled plasmas. This serves to demonstrate key aspects of the model using a familiar analytic formalism. Section III provides details of the MD simulations. Section IV presents the results of applying the model using MD simulations at strongly coupled conditions. Finally, we conclude and provide some future prospects in Sec. V.

II. WEAKLY COUPLED PLASMA

At equilibrium, the coupling strength can be quantified by the Coulomb coupling parameter

$$\Gamma = \frac{e^2/a}{k_B T}, \qquad (2)$$

which is the ratio of the Coulomb potential energy at the average interparticle spacing to the average kinetic energy. Here the coupling strength Γ is defined based on each individual species density and temperature and $\Gamma = \Gamma_e = \Gamma_i$ (Subscripts 'e' and 'i' represent electron and ion species). Properties of weakly coupled plasmas, $\Gamma \ll 1$, are well described by models based on a series of binary interactions between particles. In this section, we first revisit aspects of two- and three-body interactions that will be useful for interpreting the more complex N-body simulations in Sec. IV. We also apply the model potentials to Debye-Hückel theory, demonstrating their essential features: the separation of bound and free states and the asymptotic values of the free-charge thermodynamic state variables as α is reduced.

A. Classical bound states

Binary encounters between electrons and ions can be classified as either free or bound. Since the effective potential, $U_{\text{eff}}(r) = v_{ei}(r) + l^2/(2m_{ei}r^2)$, has a global minimum, the sign of total energy, $E = m_{ei}u^2/2 + v_{ei}(r)$, of the e-i pair determines whether the orbit is bound or free [23]. Here, $m_{ei} = m_e m_i/(m_e + m_i)$ is the reduced mass, $u = |\mathbf{v}_e - \mathbf{v}_i|$ is the relative initial particle speed, and l is the angular momentum. Figure 1 shows an example of each type of interaction for an electron-ion pair interacting via the Coulomb potential. In Figs. 1a and b, the initial conditions are such that $E > 0$ and $E < 0$ respectively, resulting in free and bound orbits.
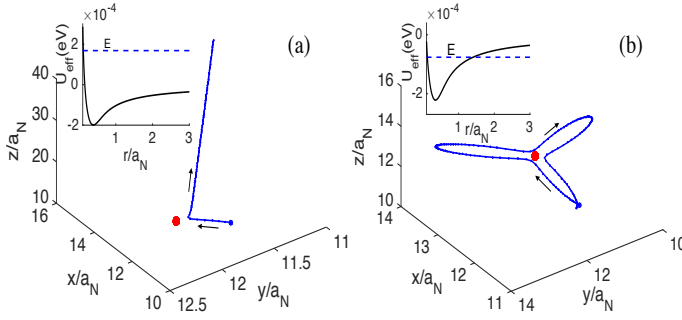
FIG. 1. Trajectories of an electron (blue) and ion (red) interacting through the Coulomb potential at conditions representing (a) free scattering and (b) a bound state. Arrows show the direction of electron motion from its starting point (blue dot). The ion to electron mass ratio is chosen to be 10^5 for this case. Distances are in units of $a_N = 10^{-5}$m.
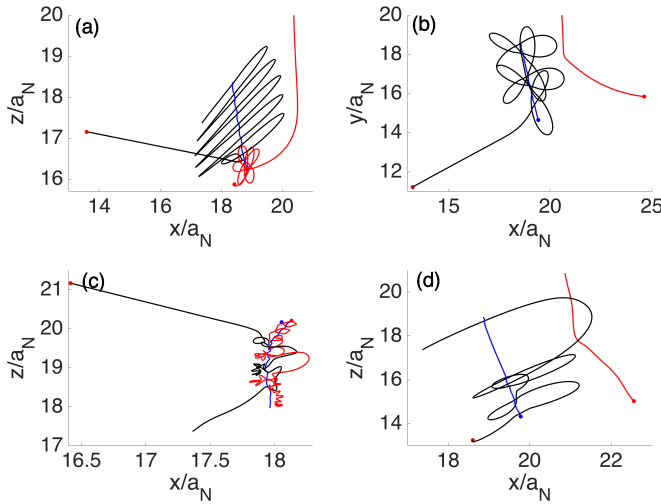

FIG. 2. Trajectories demonstrating various outcomes of three-body interactions between two electrons (red and black) and one ion (blue): (a) A classical electron-ion bound state interacts with an energetic electron, which frees the previously bound electron and forms a loosely bound state with the ion. (b) A classical electron ion-bound state interacts with an energetic electron, resulting in all free states. (c) An external electron interacts with a loosely bound state, gaining kinetic energy from the interaction and causing the bound pair to become more tightly bound. (d) An ion and two electrons all begin in a free state but form a bound pair via the three-body recombination. The ion to electron mass ratio is chosen to be 100 for this case. Distances are normalized with $a_N = 1.3366 \times 10^{-5}$m.

B. Three-body interactions

Binary collisions alone do not allow for the formation of bound states from free states, since the total energy of the binary pair is fixed. However, this can change if a third particle is present. Four types of three-body interactions are pictured in Figure 2. Figure 2d illustrates the interaction of two electrons and an ion – all

initially free – to form a bound electron-ion pair. The reduced potential energy of the newly bound pair is transferred to the second electron as additional kinetic energy. This is a classical realization of three-body recombination (3BR), which is an important heating mechanism in ultracold plasmas [13, 16, 24]. At thermal equilibrium, the formation of bound states is balanced by the reciprocal process, classical impact ionization, which is pictured in Figure 2b. The net result of these three-body interactions is that the bound pairs are less energetic than free particles, leading to overall heating of the free charges in the plasma, especially the electrons. At equilibrium, the bound subset may have a lower temperature than the free population. This will be discussed further in Sec. IV B.

C. Radial distribution functions

The radial distribution function represents the density profile surrounding individual charged particles. It is also related to the potential of mean force, which is the potential obtained when taking two particles at fixed positions and averaging over the positions of all other particles [25]

$$\mathbf{F}_{12} = \int \left[-\nabla_{\mathbf{r}_1} U(\mathbf{r}_1, \dots, \mathbf{r}_N) \right] \frac{e^{-U/k_B T}}{\mathcal{Z}} d\mathbf{r}_3 \dots d\mathbf{r}_N \quad (3)$$
$$= -k_B T \nabla_{\mathbf{r}_1} \ln g(|\mathbf{r}_1 - \mathbf{r}_2|) \equiv -\nabla_{\mathbf{r}_1} \phi(\mathbf{r}_1 - \mathbf{r}_2).$$

Here, $g(r)$ is the radial distribution function, ϕ is the potential of mean force, $\mathcal{Z} = \int \exp(-U/k_B T) d\mathbf{r}_1 \dots d\mathbf{r}_N$ is the configurational integral and $U \equiv \sum_{i,j} v(|\mathbf{r}_i - \mathbf{r}_j|)$.

In weakly coupled plasmas, the potential of mean force is the Debye-Hückel potential with a screening length equal to the total Debye length. This can be obtained using a standard fluid approach with a Boltzmann distribution of electrons and ions [26], or from the potential of mean force computed from the weakly coupled limit of the hypernetted-chain (HNC) approximation ($\phi/k_B T \ll 1$) [27]. For the bare potentials in Eq. (1), the associated weakly coupled limit of the potentials of mean force are

$$\frac{\phi_{ii}(r)}{k_B T} = \frac{\phi_{ee}(r)}{k_B T} = \frac{\Gamma}{r/a} \exp\left(-\sqrt{3\Gamma} r/a \right) \quad (4a)$$

$$\frac{\phi_{ei}(r)}{k_B T} \simeq -\frac{\phi_{ii}(r)}{k_B T} \left\{ 1 - \exp[-(r/\alpha a)^2] \right\}. \quad (4b)$$

The expression for $\phi_{ei}(r)$ relies on a scale separation between the repulsive core and screening length ($\alpha a \ll \lambda_D$). The RDFs can be obtained directly from Eq. (4) via their association with the potential of mean force $g_{ij}(r) = \exp(-\phi_{ij}/k_B T)$. Note that since both species are assumed to have the same temperature, $g_{ee} = g_{ii}$ and $g_{ei} = g_{ie}$. Figure 3 shows the RDFs for (a) electron-electron (or ion-ion) pairs with coupling strength $\Gamma = 0.02$ and $\Gamma = 0.5$ (red and blue lines respectively), (b) electron-ion pairs with $\Gamma = 0.02$ and (c) electron-ion pairs with $\Gamma = 0.5$. The electron-ion RDFs (g_{ei}) clearly show a peak
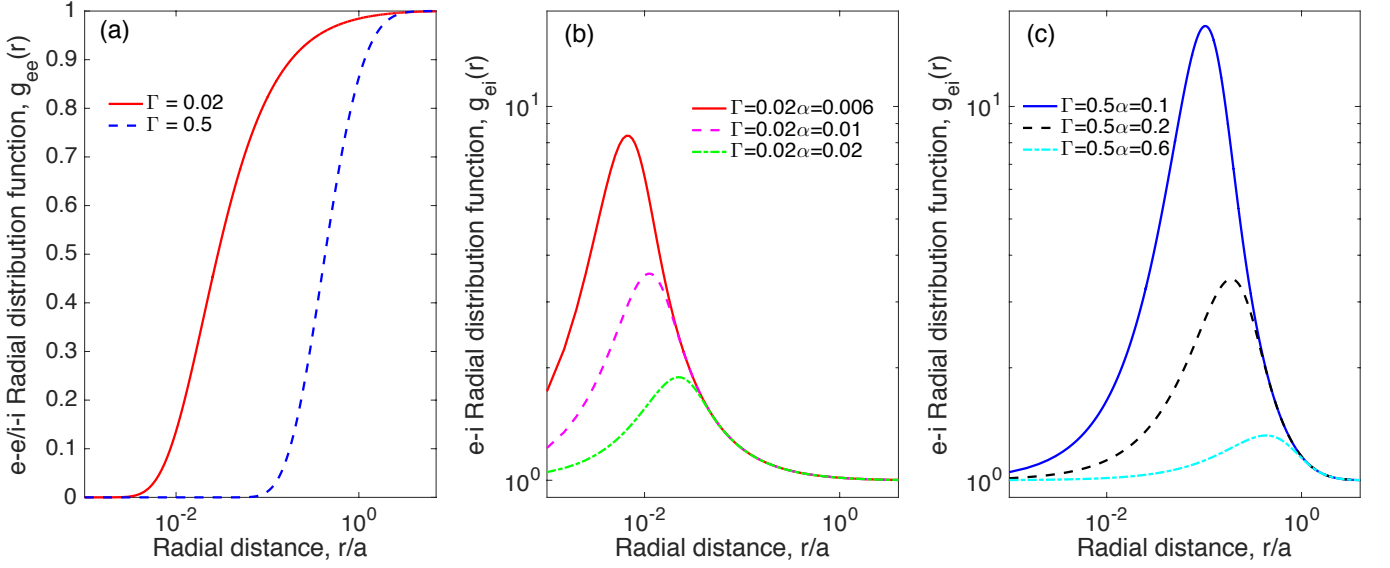
FIG. 3. Radial distribution functions at weakly coupled conditions obtained from Eq. (4). (a) Electron-electron/ion-ion RDFs for $\Gamma = 0.02, 0.5$. (b) Electron-ion RDFs for $\Gamma = 0.02$ and various α. (c) Electron-ion RDFs for $\Gamma = 0.5$ and various α. Like species RDFs ($g_{ee/ii}$) have no α dependence as they interact through the bare Coulomb potential.
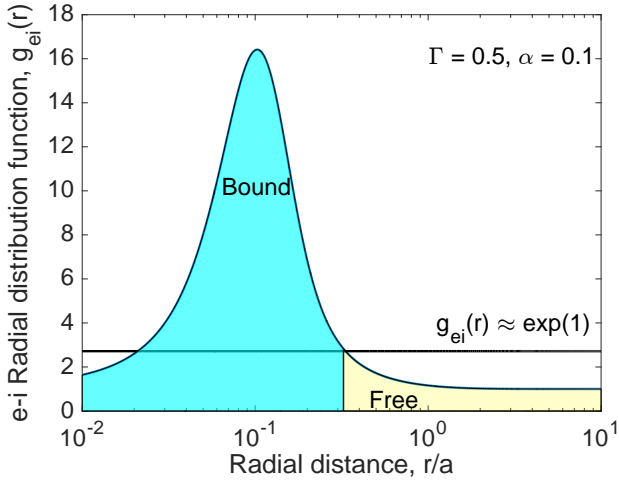

FIG. 4. Free (yellow) and bound state (cyan) contributions to $g_{ei}(r)$ with $\Gamma = 0.5$ and $\alpha = 0.1$. The horizontal and vertical lines delineate $g_{ei} = 1$ and r_c, respectively.

at the location αa with the amplitude of this peak increasing sharply either as α decreases or as the coupling strength increases. These peaks represent the classical bound states that form in the potential well at separation αa.

Next, we discuss a method to distinguish contributions due to free and bound charges in the RDFs, which will later be used to distinguish the contributions of each population to the thermodynamic state variables. As discussed in Sections II A and II B, the condition for an e-i pair to be bound is $E < 0$, which can occur as the result of interaction with a third particle. In a many-body picture, the potential of mean force models the average

interaction energy of an e-i pair in the presence of the surrounding plasma. Applying this to the condition for bound states from Sec. II B suggests that particle interactions for which $|\phi_{ei}(\mathbf{r}_{12})| > k_B T$ are expected to be bound and those with $|\phi_{ei}(\mathbf{r}_{12})| < k_B T$ free on average. We use this as a criterion to separate $g_{ei}(r)$ into free and bound contributions according to

$$\max\{g_{ei}^{\text{free}}\} = \exp(1) . \tag{5}$$

In other words, a critical distance r_c defined by $|\phi_{ei}(r_c)| = k_B T$ delineates a separation between bound and free populations: Particles in the region $r > r_c$ are considered free and those with $r < r_c$ bound. Figure 4 provides an example for $\Gamma = 0.5$ and $\alpha = 0.1$, showing the separation between bound and free contributions to the radial density profile.

Equation (5) provides a phenomenological ansatz which makes a sharp division between free and bound contributions and does not include any statistical variation. A more realistic model would include a transition region of a certain width. For example, there might be several pairs of opposite charges not bound even when their kinetic energy is less than their average potential energy and vice-versa. Such a statistical width would be expected to lead to a variation in thermodynamics quantities being estimated based on criterion Eq. (5). This will be discussed further in subsections IV D and IV E.

The bound state fraction can be estimated directly from the e-i RDFs by taking the ratio of the number of bound particles to the total number of particles

$$X_b = \frac{\int_0^{r_c} [g_{ei}(r) - 1] \, d\mathbf{r}}{\int_0^{\infty} [g_{ei}(r) - 1] \, d\mathbf{r}} . \tag{6}$$
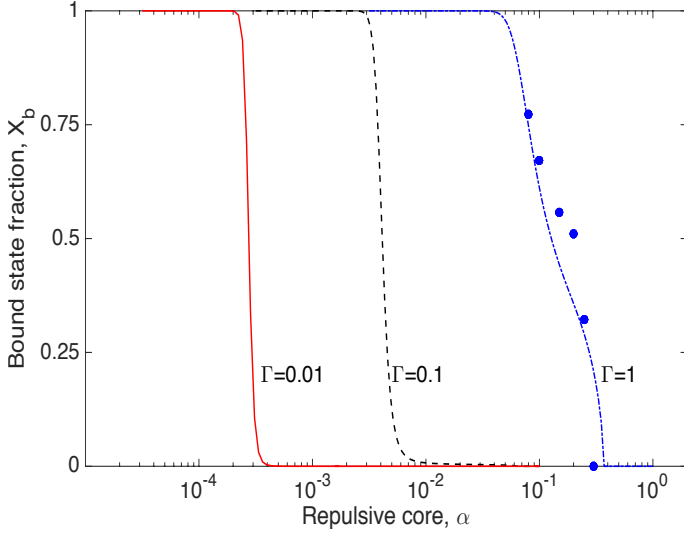
FIG. 5. Fraction of bound states with respect to repulsive core parameter α obtained from Eqs. (5) and (6). The lines use g_{ie} from Debye-Hückel theory, Eq. (4), and filled blue circles use g_{ie} from MD simulations for $\Gamma = 1$.

Where X_b is the bound state fraction of the total system of particles. Figure 5 illustrates how the fraction of bound states varies with the repulsive core parameter α. At a given coupling strength, there is a transition regime where the bound state fraction increases sharply. The upper edge of this region indicates a nearly recombined plasma (i.e., classical neutral gas) while the lower edge indicates a fully ionized plasma. The transition is observed to occur when $\alpha \simeq 0.05\Gamma$ based on this data in the range $\Gamma = 0.01 - 1$.

D. Excess pressure

At equilibrium, the pressure can be computed directly from the RDFs. It consists of an ideal component and an excess component: $P = P_{\text{ideal}} + P_{\text{ex}}$, where $P_{\text{ideal}} = nk_BT$, and the excess pressure is [25, 28]

$$P_{\text{ex}} = -\frac{2}{3}\pi \sum_{i,j} n_i n_j \int_0^\infty v'_{ij}(r)g_{ij}(r)r^3 dr , \quad (7)$$

where v'_{ij} denotes the radial derivative of the bare potentials.

Figure 6a shows how the excess pressure P_{ex} varies with α for three values of Γ. Based on these curves, we identify three parametric regions. In the rightmost region III, the repulsive core scale length is larger than the average particle separation ($\alpha \geq 1$). Here, the long-range nature of the repulsive cores generates a significant positive excess pressure. A physical example of this regime is dense degenerate plasmas where the de Broglie wavelength exceeds the average interparticle spacing. In the leftmost region I, the repulsive core length scale is much
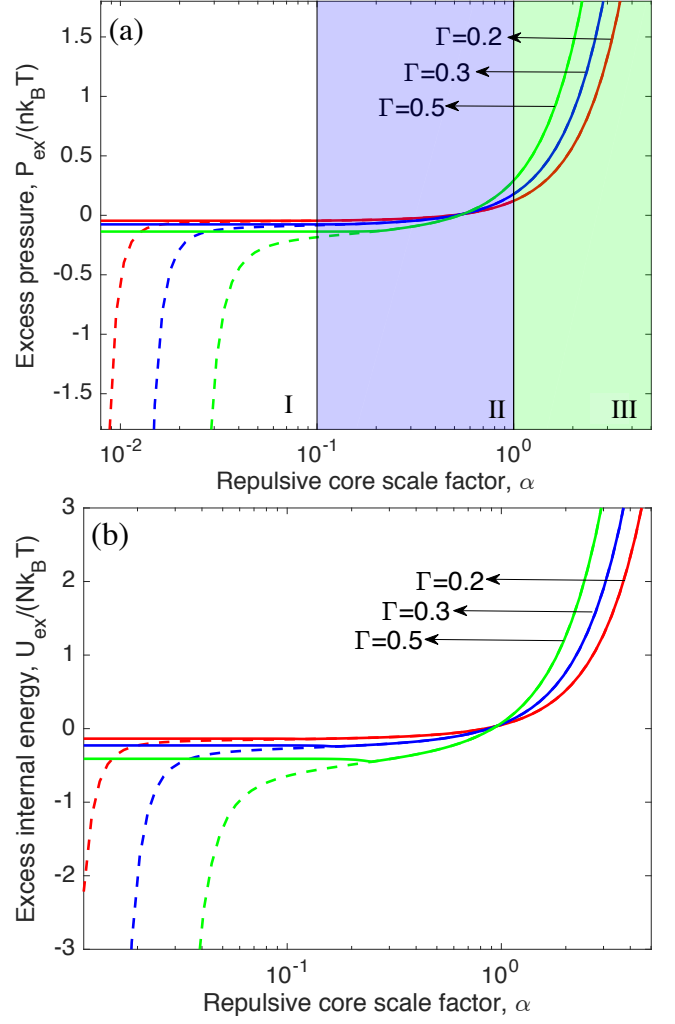

FIG. 6. (a) Excess pressure for weakly coupled conditions calculated from Eqs. (1), (4), and (7). (b) Excess internal energy variation with α and Γ using Eq. (4). In each, dashed lines are for the combined free-plus-bound system. Solid lines contain just the free-charge contribution.

smaller than the average particle spacing ($\alpha \ll 1$). Here, the electron-ion potential well is very deep, leading to significant recombination and a corresponding negative excess pressure. This is the region of interest for modeling ultracold neutral plasmas. In the intermediate region II, the excess pressure takes a constant value that is slightly negative but larger than -1, indicating that the total pressure remains positive in this regime.

The solid lines in Fig. 6a show the contribution to the excess pressure associated with free charges, which was obtained using the energy criterion in Eq. (5). Although the excess pressure diverges toward large negative values when the bound states are kept (dashed lines), it is found to be independent of the repulsive core scale parameter α when they are removed (solid lines). The asymptotic value associated with the free charge population corresponds to that of the intermediate region II.
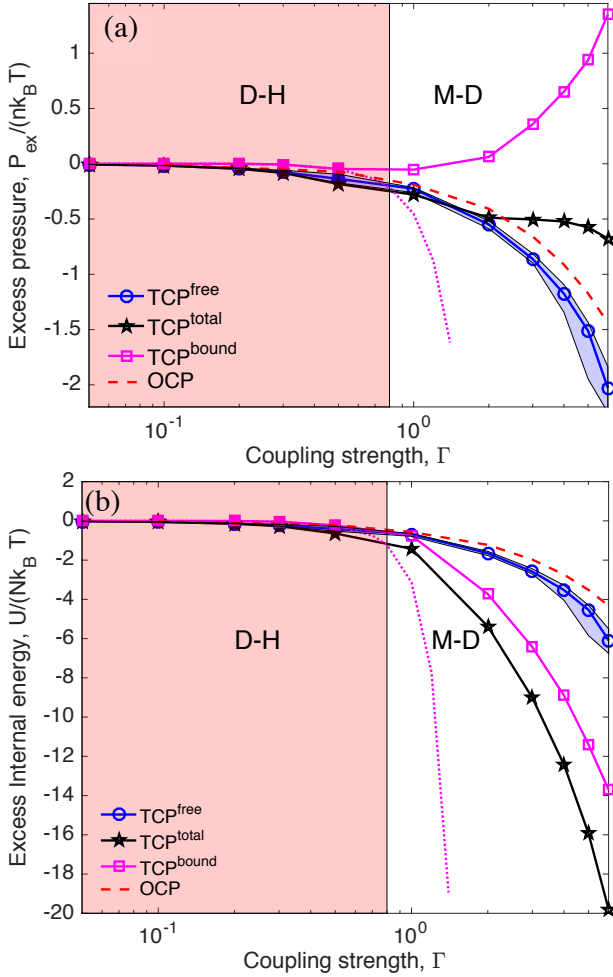
FIG. 7. Dependence on Γ of (a) the excess pressure and (b) excess internal energy at $\alpha = 0.1$. Black lines with stars are for the total (bound plus free) system, blue lines with circles are just the free charge contributions, and the magenta line with squares indicates the bound state contributions only. Red dashed lines are the OCP values. Shaded regions indicate where the thermodynamic state variables are calculated using RDFs obtained from Debye-Hückel description, while unshaded regions contain molecular dynamics results. Dotted lines represent an extension of Debye-Hückel theory into the strongly coupled regime. The blue shaded regions show how the excess pressure and internal energy of the free charges varies when the R.H.S. of Eq. 5 is varied from $\exp{(0.5)}$ to $\exp{(2)}$.

This asymptotic value is the partial excess pressure associated with the free charge population. The αa value separating this intermediate region from region I is associated with the spatial location where the potential energy of the attractive Coulomb interaction significantly exceeds the average kinetic energy.

In a typical electron-ion radial distribution function, the peak associated with bound state contributions increases several orders of magnitude as αa varies from higher values of $\alpha a \sim 1$ to short ranged values $\alpha a \ll 1$ (see Fig. 11c). If we consider the influence of a statistical

variation in the value used to define the bound population in the exponent of Eq. (5), we find that the result for the partial excess pressure associated with each contribution (free or bound) is insensitive to the particular value chosen. For example, considering a range from $e\phi/k_BT = 0.5$ to 2, the corresponding $g(r_c)$ value at the cutoff will vary from 1.6 - 7.4. A change in cutoff over this range of values has a negligible influence on the asymptotic value of the partial excess pressure of the free charges shown in Fig. 6. This aspect will be discussed and quantified further in subsections IV D and IV E.

In our model, α is a set parameter that is not associated with a physical scale. However, consider for a moment associating the thermal de Broglie wavelength with the repulsive core scale length. The ratio of the thermal de Broglie wavelength and the interparticle spacing $\lambda_{db}/a = [2\pi\hbar^2/(m_{ie}k_BT)]^{1/2}/a$ is a measure of the influence of quantum mechanical wave effects of the ion fluid. Here, $m_{ie} = m_em_i/(m_e+m_i) \simeq m_e$ is the reduced mass. Applying $\alpha a = \lambda_{db}$, provides $\Gamma a/\lambda_{db} \simeq 2/\sqrt{T[\text{eV}]}$. Thus, the boundary $\alpha = \lambda_{db}/a \simeq 0.05\Gamma$ is simply associated with the temperature $T \simeq 0.01$ eV. If $T \lesssim 0.01$ eV, the plasma is in region I and the excess pressure is highly negative, indicating the system will collapse (i.e., recombine). If $T \gtrsim 0.01$ eV, the plasma is in the plateau region II with a small negative excess pressure, but a positive total pressure. Ultracold plasmas fall deep in region I. The additional challenge at strong coupling ($\Gamma \gtrsim 1$) is that the intermediate region becomes narrow, and the Debye-Hückel approximation breaks down. In this region, we will separate the contributions from free charges (plasma) and classical bound states using the same methods outlined in this section, but apply them to RDFs calculated with MD simulations.

Figure 7a shows the excess pressure dependence on Γ at a fixed value of $\alpha = 0.1$. Data in the shaded regions was obtained using the Debye-Hückel model and data in the non-shaded regions was obtained using molecular dynamics simulations. The black line with pentagram markers shows the total excess pressure including free and bound states. The blue line with circles denotes the excess partial pressure of the free charges. The magenta line with square markers represents bound state contribution. At weak coupling, the excess pressure is small, but grows significant as strong coupling is approached. The role of free and bound contributions to the excess pressure in the strongly coupled regime will be further in Sec. IV D.

E. Internal energy

The same arguments used to describe excess pressure in the previous section can be carried over to describe excess internal energy. The excess internal energy for an electron-ion plasma can be written in terms of the RDFs
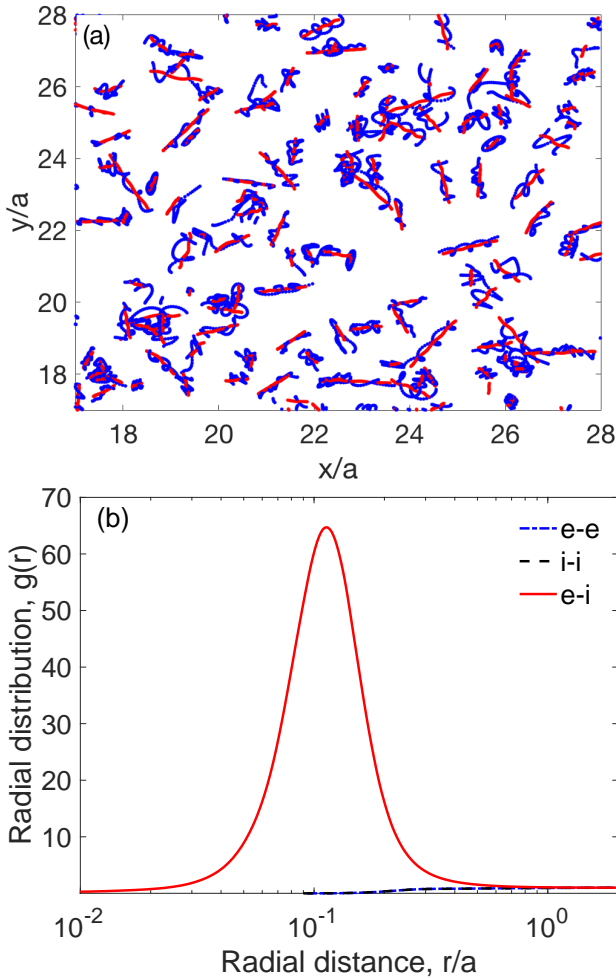
FIG. 8. (a) Bound state trajectories of electron-ion pairs during a simulation with $\Gamma = 1$ and $\alpha = 0.1$ over a time interval of $3\omega_{pe}^{-1}$. The free particle trajectories have been removed. (b) The RDFs at the same conditions, showing the peak in $g_{ei}(r)$ at $r = \alpha a$.

as [28]

$$\frac{U_{ex}}{N} = \frac{2\pi}{n} \sum_{i,j} n_i n_j \int_0^\infty g_{ij}(r) \left(v_{ij}(r) - T\frac{\partial}{\partial T} v_{ij}(r) \right) r^2 dr .$$
(8)

Here N is the total number of particles in the system of volume V such that $n = N/V$. Note that in the present context α is constant, so the interaction potentials v_{ij} are independent of temperature and the second term in Eq. (8) is zero. However, in a dense plasma context $\alpha a \simeq \lambda_{\rm db}$, so the interaction potentials depend on temperature and this term would be nonzero.

Fig. 6b shows the variation of internal energy with the repulsive core parameter α for different values of coupling strength Γ. As was the case with the excess pressure, the internal energy of the full system (free plus bound) diverges sharply as α decreases, but it asymptotes to a constant when the bound state contribution is removed.

We emphasize that a well-defined thermodynamic pressure and energy for weakly coupled plasmas traditionally rely on being able to neglect the inter-particle interactions in comparison with their kinetic energy. The analysis of this section illustrates that the inherent difficulties of a point-particle description of a plasma are still formally present at weak coupling, as evidenced by the negative divergence of the pressure and energy as $\alpha \to 0$. In practice, quantum mechanical effects preventing Coulomb collapse at close distances are responsible for the stability of matter [29].

III. SIMULATION METHOD

Three dimensional classical MD simulations were carried out using the open source code LAMMPS [30]. LAMMPS is massively parallel (both CPU and GPU based) and is efficient for large-scale particle simulations. The simulation geometry was a 3D cubic box with periodic boundary conditions. Each simulation used 10^4 electrons and 10^4 ions, and the typical time step was $0.005\omega_{pe}^{-1}$. These parameters were chosen to ensure energy conservation as well as to fully resolve the dynamics of the lightest species (i.e. electron) during the simulation [31]. Simulations were conducted by first equilibrating the system using a Nosé-Hoover thermostat to achieve a desired temperature corresponding to a particular Γ value [20]. The temperature of each species s at each timestep was calculated from $\frac{3}{2}N_s k_B T_s = \frac{1}{2}m_s \sum_i^{N_s} v_{si}^2$, where v_{si} is the instantaneous particle velocity. After equilibrium was achieved, the thermostat was turned off and the RDF was computed. The PPPM (particle-particle, particle-mesh) method [32] was used to calculate the long range interactions. The interaction potentials used were those from Eq. (1), with α an input parameter. The ion mass was taken to be 10 times the electron mass. However, here we present results at equilibrium, in which case we found that the mass ratio did not influence the RDFs, as expected from classical equilibrium statistical mechanics.

These simulations were limited to values of α no less than 0.1 due to energy conservation requirements. We found that at smaller values of α it became prohibitive to resolve the timescales of tightly bound pairs to the degree required for energy conservation. Nevertheless, this value was small enough to reach the desired plateau regime.

IV. STRONGLY COUPLED PLASMA

We now apply the concepts and techniques discussed in Section II to moderately and strongly coupled plasmas using classical MD simulations.
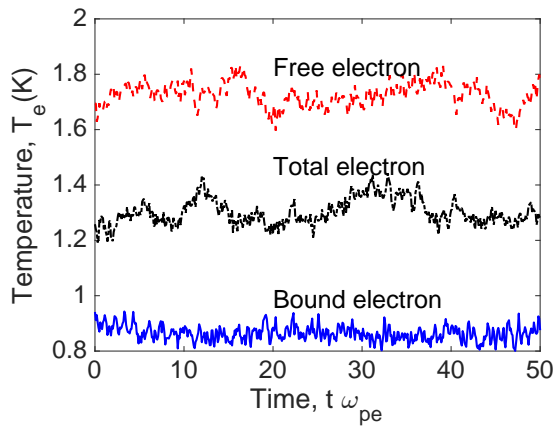
FIG. 9. Electron temperature for free (red dashed line) and bound (blue line) species in a simulation with $\Gamma = 1$ and $\alpha = 0.1$. The black line shows the total electron temperature in the system.
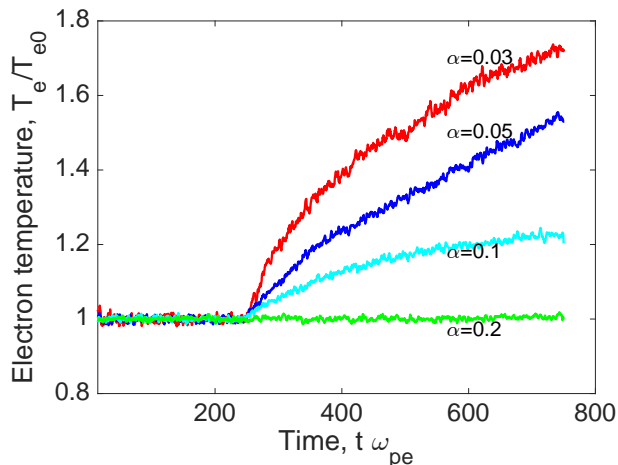

FIG. 10. The evolution of the electron temperature in an ultracold plasma simulation at $\Gamma = 10$ and various values of α. The heating rate increases as the repulsive core distance αa shrinks. The system is kept under the thermostat for the first $250\ \omega_{pe}^{-1}$ and then lifted to allow free temperature evolution.

A. Classical bound states

Compared to a weakly coupled plasma, a strongly coupled plasma whose particles interact through the pair potentials of Eq. (1) is expected to form more bound states. This is because the depth of the electron-ion potential well scales linearly with Γ. Indeed, comparing Fig. 8b to Fig. 4, doubling Γ yields nearly a factor of four increase in the peak value of $g_{ei}(r)$ for the same value of α, indicating that a larger fraction of the plasma is confined to tight orbits like those pictured in Fig. 8a. In addition to the many binary bound pairs, we observed that clusters of bound pairs can form stable structures under strong coupling conditions. These can take the form of long chains, or rings. These structures will be discussed in more detail in a later work.

In the present studies we limit our results up to moderate coupling strengths only. The reason is that as we move towards stronger coupling strength, the system's increased affinity for forming bound states results in a "plasma" that is primarily composed of clumped bound pairs. Removal of the bound states would then effectively take the majority of charged particles out of evaluation of thermodynamic properties, reducing the effective coupling strength of the free charges below their nominal Γ value. Thus our simulation results will not remain practical for higher Γ values. Physically, this is related to the rapid rate of recombination at these conditions.

B. Three-body interactions

MD simulations permit us to investigate the cumulative effect of the three-body interactions studied in isolation in Section II B. To do so, we used a microscopic criterion (instead of Eq. (5)) to classify individual electron-ion pairs as either free or bound. This method was only used for the purpose of getting the data for Figure 9. For a selected pair of particles, we computed $U_{\text{eff}}(r)$ and E as though the two particles' motion were unaffected by the surrounding plasma. Repeating for many such pairs, we calculated the kinetic energy for the population of free electrons and bound electrons. The results for $\Gamma = 1$ and $\alpha = 0.1$ are plotted in Figure 9. This shows that free electrons carry approximately twice as much kinetic energy than those bound to an ion for this set of parameters. This is in agreement with our expectations from the three-body dynamics described in Section II B, where electrons that end up in a bound state were observed to give up kinetic energy to other nearby electrons via scattering. Figure 9 also shows that the two electron populations' temperatures remain fixed (aside from fluctuations). This indicates that not only is the system as a whole in equilibrium, but the free and bound electron sub-systems have each attained their own thermal equilibrium.

We also find that if the thermostat is lifted, the plasma will heat; as evidenced by the temperature evolution plots in Figure 10. It can be seen that when the thermostat is switched off at time $t \approx 250\omega_{pe}^{-1}$, the electron temperature increases rapidly if α is sufficiently small. Only the electron temperature is shown because the ion temperature curves are identical. The heating rate increases as α decreases, implying that the heating of the system arises from the liberation of Coulomb potential energy via classical three-body recombination. At sufficiently large values of α, the heating effect is insignificant even after removing the thermostat, as in the $\alpha = 0.2$ line of Figure 10, as well as the for the parameters of Figure 9. However, for smaller values of α, the heating effects become more and more significant because the deeper potential well in the electron-ion interaction provides a larger potential energy source that is converted to kinetic energy via heating. This figure demonstrates the
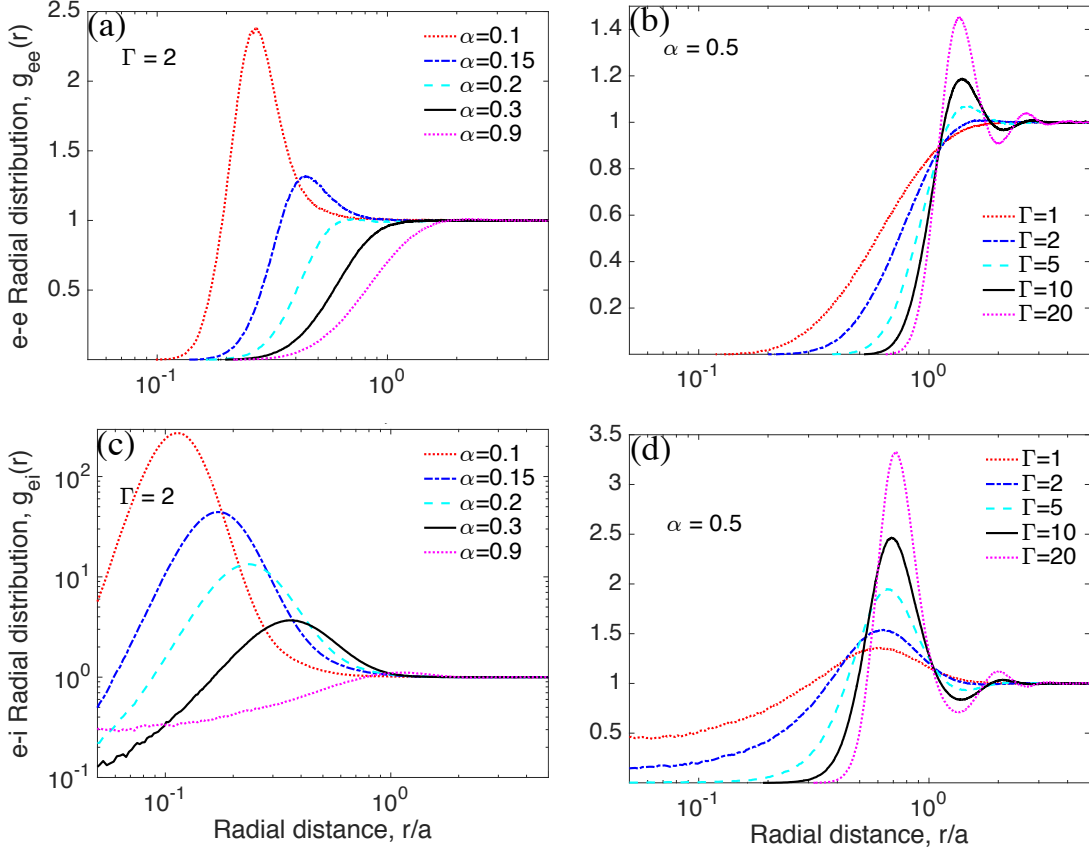
FIG. 11. Radial distribution functions $g_{ee}(r)$ (top) and $g_{ei}(r)$ (bottom) for equilibrium electron-ion plasma, showing variation with α (left) and Γ (right).

rapid evolution of ultracold plasmas, and that the concept of quasi-equilibrium relates to a narrow time window. In contrast, the same concept is much more clearly defined in dense degenerate plasmas with slow recombination rates [28, 33].

We note that the use of particle trajectories to separate free and bound charges is used only in the temperature calculations of this subsection. There are three reasons: 1) it is computationally expensive; 2) bound pairs tend to be difficult to track because they survive only a few plasma periods before being broken up; 3) at higher coupling, the binary encounter picture is inappropriate, since bound pairs tend to clump and form complex structures. For these reasons, the remainder of the thermodynamics results in this section are based on the bound/free separation criterion Eq. 5 as discussed further below.

C. Radial distribution functions

Figure 11 shows the RDFs for electron-electron and electron-ion pairs obtained from classical MD simulation of an ultracold plasma. The upper panels show the RDFs for electron-electron pairs while the lower panel shows the RDFs for electron-ion pairs. Subplots (a) and (c)

show the effect of varying α at fixed Γ, and vice-versa for subplots (b) and (d).

In addition to the peak in $g_{ei}(r)$ near $r = \alpha a$, the figures show an additional peak in $g_{ee/ii}(r)$. This feature of the like-charge RDFs is a consequence of the system's tendency to cluster. Tightly bound e-i pairs are essentially dipoles, which attract other dipoles and cause clumping to occur. This permits, for example, two bound electrons to lie near each other in spite of their mutual repulsion.

Though interesting, this secondary peak in $g_{ee/ii}(r)$ complicates the procedure for separating bound and free populations at the RDF level. In order to use Eq. (5) to remove bound states from $g_{ei}(r)$, we must also remove them from $g_{ee/ii}(r)$ in an internally consistent way. To do so, we first enforce Eq. (5) as before, yielding a cutoff distance $r_{c,ei}$. Next, we determine a second cutoff distance $r_{c,ii}(= r_{c,ee})$ that maintains quasineutrality within the individual bound and free subpopulations. That is, we determine $r_{c,ii/ee}$ such that

$$4\pi n_i \int_{r_{c,ii}}^{\infty} g_{ii}(r) r^2 dr - 4\pi n_e \int_{r_{c,ei}}^{\infty} g_{ei}(r) r^2 dr = -1 \quad (9a)$$

$$4\pi n_i \int_{r_{c,ei}}^{\infty} g_{ei}(r) r^2 dr - 4\pi n_e \int_{r_{c,ee}}^{\infty} g_{ee}(r) r^2 dr = 1. \quad (9b)$$
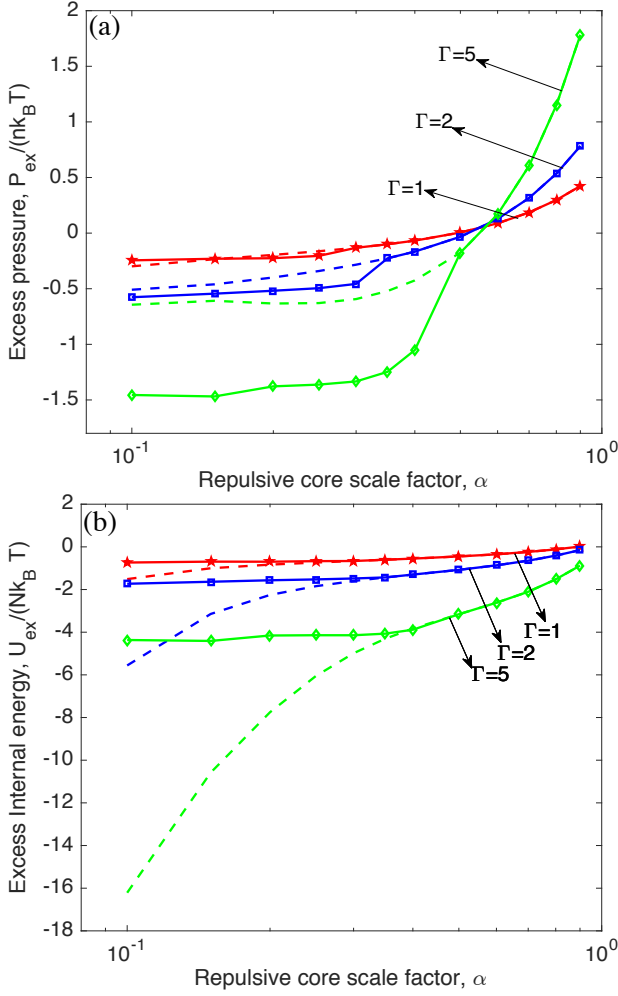
FIG. 12. Dependence of the excess pressure (a) and excess internal energy (b) on the repulsive core parameter α at various coupling strengths. Dashed lines indicate results for the combined free-plus-bound system and the solid lines with markers indicated results isolating the free-charge components of the system.

Again, the hypothesis here is that approximately all contributions to $g_{ii}(r)$ below $r_{c,ii}$ are due to clustering of bound pairs.

D. Excess pressure

The excess pressure for moderately coupled ultracold plasmas was evaluated using Eq. (7). The input RDFs for these moderately coupled media were obtained from equilibrium MD simulations. In Fig. 12a, the total excess pressure (including both free and bound charges) is plotted as a function of α for $\Gamma = 1, 2, 5$. The line plots with markers show the excess pressure calculated after removal of bound states from the RDFs. The bound- and free-state RDFs have been separated using Eqs. (5) and (9). Like the weakly coupled regime from Fig. 6, the

excess pressure for the free charge population is found to plateau to an α-independent value for small α. Molecular dynamics simulations become computationally challenging due to energy conservation issues for small values of the parameter α (less than $\alpha = 0.1$). This limits the accessible range of α and is the reason the pressure shown in Fig. 12a does not reach the divergent regime at smaller α seen in the weakly coupled study (Fig. 6a).

Fig. 7a shows the excess pressure dependence on Γ with α fixed at a value of 0.1. The pressure of the total plasma remains positive ($P_{ex} > -1$) at all values of Γ shown. The blue line with circles and magenta line with squares are the partial excess pressures due to free and bound charges, respectively. This figure shows that the partial excess pressure due to the free charge contribution closely follows the OCP results, i.e., $P_{ex} < 0$ and that the total partial pressure associated with the free charges becomes negative around $\Gamma \approx 4$. The collapsing nature of free electron-ion gas is responsible for this negative excess pressure. The partial excess pressure due to bound states is always found to be positive, much like what one would expect for a gas of neutral atoms. As the coupling strength increases, a large fraction of plasma forms bound states and hence they contribute more to keep the total excess pressure positive. The figure also shows that the MD results show a consistent trend that merges with the Debye-Hückel results at weak coupling.

We have also tested the robustness of the criterion in Eq. (5) by varying the value in the exponent representing $e\phi/k_B T$, from 0.5 to 2. This window represents statistical uncertainty in the boundary separating free and bound populations. In other words, this variation in $e\phi/k_B T$ provides an approximate statistical width to the critical cutoff distance r_c which is used to separate free and bound states from an electron-ion radial distribution function. The shaded region in Fig. 7a shows the variation in excess pressure for free charges as we vary the value of exponent $e\phi/k_B T$ of criterion in Eq. (5). The small width of this shaded region suggests that the results do not change significantly. Thus we conclude that the physics-based argument for the criterion $e\phi/k_B T \sim 1$ and the insensitivity of results to the particular value chosen provides additional confidence in the robustness of this method.

E. Internal energy

The excess internal energy was also evaluated using the RDFs obtained from MD along with Eq. (8). Figure 12b shows how the excess internal energy of the total (free plus bound) plasma depends on α at $\Gamma = 1, 2, 5$. The lines with markers represent the excess internal energy of free charges found by removing the contribution of bound states to $g_{ij}(r)$. Similarly to previous results for excess pressure, the removal of bound states again leads to values of U_{ex} that are independent of α in the $\alpha \to 0$ limit.

Fig. 7b shows the excess internal energy at different values of coupling strength Γ with $\alpha = 0.1$. Similar to excess pressure, the excess internal energy of the free states (blue line with stars) is close to the OCP value (red dashed line). At increased coupling strength, an increase in the bound state fraction causes the internal energy to become increasingly negative. Similar to subsection IV D, the partial excess internal energy for free charges includes a shaded region representing the results obtained as the value of the exponent $e\phi/k_BT$ in Eq. (5) ranges from 0.5 to 2. Again, the small width in the variation of the excess pressure due to free charges suggests that the criterion used in Eq. (5) is insensitive to statistical variations in deciding the critical cutoff distance r_c in electron-ion radial distribution functions.

V. CONCLUSIONS

Using Debye-Hückel theory for the weakly coupled regime and equilibrium MD simulations for the strongly coupled regime, we observed that the Coulomb collapse of a classical electron-ion plasma can be prevented by applying a repulsive core force at close distance (αa) in the electron-ion interaction. Furthermore, the removal of the bound state contribution to the radial distribution functions was shown to provide predictions for the thermodynamic state variables that are independent of the model repulsive core length scale.

These results provide a method to separate the contribution of free charges from classical bound states in the evaluation of pressure and internal energy of a classical electron-ion plasma. This enables quasi-equilibrium analysis of classical electron-ion plasmas, as are found in ultracold neutral plasma experiments (Γ_i up to 5 and Γ_e up to 0.1). Such an analysis is useful for connecting theoretical predictions, which are made at fixed conditions, with experimental measurements, which are made over short enough time intervals that the conditions may be considered fixed. The work lays important groundwork for the further development of two-component models for ultracold plasmas based on a classical point-particle picture of the microscopic dynamics. Future work will extend our studies to a two-temperature electron-ion system, which is closer to the conditions of an ultracold neutral plasma experiment. This study was also limited to moderate coupling strengths due to the formation of complex bound-state structures at higher coupling strengths. Future studies will investigate these structures in further detail.

[1] A. Diaw and M. S. Murillo, Phys. Rev. E **92**, 013107 (2015).

[2] T. S. Strickler, T. K. Langin, P. McQuillen, J. Daligault, and T. C. Killian, Phys. Rev. X **6**, 021021 (2016).

[3] R. Drake, *High-Energy-Density Physics: Fundamentals, Inertial Fusion, and Experimental Astrophysics*, Shock Wave and High Pressure Phenomena (Springer Berlin Heidelberg, 2006).

[4] R. Redmer and G. Röpke, Contributions to Plasma Physics **50**, 970 (2010).

[5] K. A. Brueckner and S. Jorna, Rev. Mod. Phys. **46**, 325 (1974).

[6] M. Baus and J.-P. Hansen, Physics Reports **59**, 1 (1980).

[7] M. Baus, Journal of Physics A: Mathematical and General **11**, 2451 (1978).

[8] M. Bonitz, B. B. Zelener, B. V. Zelener, E. A. Manykin, V. S. Filinov, and V. E. Fortov, Journal of Experimental and Theoretical Physics **98**, 719 (2004).

[9] T. C. Killian, S. Kulin, S. D. Bergeson, L. A. Orozco, C. Orzel, and S. L. Rolston, Phys. Rev. Lett. **83**, 4776 (1999).

[10] T. C. Killian, Science **316**, 705 (2007).

[11] T. Killian, T. Pattard, T. Pohl, and J. Rost, Physics Reports **449**, 77 (2007).

[12] F. Robicheaux and J. D. Hanson, Phys. Rev. Lett. **88**, 055002 (2002).

[13] T. C. Killian, M. J. Lim, S. Kulin, R. Dumke, S. D. Bergeson, and S. L. Rolston, Phys. Rev. Lett. **86**, 3759 (2001).

[14] L. Guo, R. H. Lu, and S. S. Han, Phys. Rev. E **81**, 046406 (2010).

[15] S. G. Kuzmin and T. M. ONeil, Physics of Plasmas **9**, 3743 (2002).

[16] S. G. Kuzmin and T. M. O'Neil, Phys. Rev. Lett. **88**, 065003 (2002).

[17] S. Mazevet, L. A. Collins, and J. D. Kress, Phys. Rev. Lett. **88**, 055001 (2002).

[18] V. E. Fortov and I. Iakubov, *The Physics of Non-ideal Plasma* (World Scientific, 2000).

[19] I. Klimontovich, *The statistical theory of non-equilibrium processes in a plasma*, International series of monographs in natural philosophy (M.I.T. Press, 1967).

[20] D. J. Evans and B. L. Holian, The Journal of Chemical Physics **83**, 4069 (1985).

[21] C. Deutsch, Physics Letters A **60**, 317 (1977).

[22] G. Kelbg, Annalen der Physik **467**, 354 (1963).

[23] J. Taylor, *Classical Mechanics* (University Science Books, 2004).

[24] R. S. Fletcher, X. L. Zhang, and S. L. Rolston, Phys. Rev. Lett. **99**, 145001 (2007).

[25] T. Hill, *An Introduction to Statistical Thermodynamics*, Dover Books on Physics (Dover Publications, 2012).

[26] F. Chen, *Introduction to plasma physics* (Plenum Press, 1974).

[27] S. D. Baalrud and J. Daligault, Physics of Plasmas **21**, 055707 (2014).

[28] J. P. Hansen and I. R. McDonald, Phys. Rev. A **23**, 2041 (1981).

[29] E. H. Lieb, Rev. Mod. Phys. **48**, 553 (1976).

[30] S. Plimpton, Journal of Computational Physics **117**, 1 (1995).

[31] G. Dimonte and J. Daligault, Phys. Rev. Lett. **101**, 135001 (2008).

[32] S. Plimpton, R. Pollock, and M. Stevens, in *Proceedings of the Eighth SIAM Conference on Parallel Processing for Scientific Computing* (1997).

[33] J. N. Glosli, F. R. Graziani, R. M. More, M. S. Murillo, F. H. Streitz, M. P. Surh, L. X. Benedict, S. Hau-Riege, A. B. Langdon, and R. A. London, Phys. Rev. E **78**, 025401 (2008).